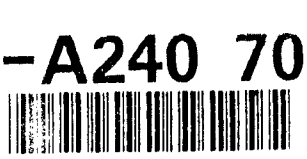

NASA Contractor Report 187606
ICASE Report No. 91-60

ICASE

SIMULATION OF TRANSIENT FLOW IN A SHOCK TUNNEL AND A HIGH MACH NUMBER NOZZLE

P. A. Jacobs

Contract No. NAS1-18605
July 1991

Institute for Computer Applications in Science and Engineering
NASA Langley Research Center
Hampton, Virginia 23665-5225

Operated by the Universities Space Research Association

NASA
National Aeronautics and
Space Administration

Langley Research Center
Hampton, Virginia 23665-5225

SIMULATION OF TRANSIENT FLOW IN A SHOCK TUNNEL AND A HIGH MACH NUMBER NOZZLE

P. A. Jacobs[1]
Institute for Computer Applications in Science and Engineering
NASA Langley Research Center, Hampton, VA 23665

ABSTRACT

A finite-volume Navier-Stokes code was used to simulate the shock-reflection and nozzle starting processes in an axisymmetric shock tube and a high Mach number nozzle. The simulated nozzle starting processes were found to match the classical quasi-one-dimensional theory and some features of the experimental measurements. The shock-reflection simulation illustrated a new mechanism for the driver-gas contamination of the stagnated test gas.

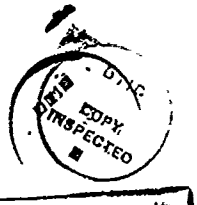

Accession For	
NTIS GRA&I	☑
DTIC TAB	☐
Unannounced	☐
Justification	
By	
Distribution/	
Availability Codes	
Dist	Avail and/or Special
A-1	

[1]Research was supported by the National Aeronautics and Space Administration under NASA Contract No. NAS1-18605 while the author was in residence at the Institute for Computer Applications in Science and Engineering (ICASE), NASA Langley Research Center, Hampton, VA 23665.

1 INTRODUCTION

Free-piston driven reflected-shock tunnels have been one of the most successful types of impulse facilities [1] and have been able to provide a versatile range of hypervelocity test conditions with reasonable test-time durations. However, little is known of the detailed flow processes that are involved with their operation because, in the past, the unavailability of large computing resources has limited most analyses to either steady-state in two dimensions (as in nozzle design [2]) or to time-dependent simulation in one dimension (as in shock tube performance estimates [3] or nozzle starting estimates [4]). Recent studies have begun to investigate multidimensional transient effects such as the shock interactions in the throat region [5], axisymmetric nozzle starting times [6] and flow establishment over aerodynamic models [7]. This paper will study, via time-accurate numerical simulation, the shock reflection and the nozzle starting process in an axisymmetric shock tube and a high Mach number nozzle.

1.1 REFLECTED-SHOCK TUNNEL OPERATION

The principal features of a free-piston driven shock tunnel, along with an approximate wave diagram, are shown in Fig. 1. The driver (or compression) tube, which initially contains low pressure driver gas downstream of the piston, and the shock tube which contains the test gas, are separated by the (strong) primary diaphragm. Attached to the downstream end of the shock tube is the facility nozzle whose throat is significantly smaller than the inside diameter of the shock tube. The subsonic portion of the nozzle effectively closes the downstream end of the shock tube and forms the shock reflection region. The supersonic portion of the nozzle empties directly into a test section and dump tank which is evacuated to an initial pressure of approximately 30 Pa. The test gas is retained in the shock tube by a (thin mylar) secondary diaphragm.

The first stage of operation consists of the launch of the piston and its acceleration along the compression tube. The driving force is supplied by compressed air from a reservoir. The driver gas in front of the piston is compressed and eventually bursts the primary diaphragm. After diaphragm rupture, the driver gas expands into the shock tube and shock-compresses the test gas before it. The *primary* shock wave travels the length of the shock tube, reflects from the closed end, and brings the test gas to rest in the nozzle supply region.

Upon shock reflection, the light secondary diaphragm bursts and some of the test gas following the primary shock expands through the nozzle throat into the divergent part of the nozzle. From the point of view of the nozzle, the shock tube is now a reservoir of (nearly) stagnant, high-temperature, high-pressure test gas. The Mach 8 contoured nozzle discussed in this paper is large enough for the starting time to significantly reduce the available test time. Thus, it was hoped that a direct simulation of the multidimensional flow processes would help identify the mechanism(s) delaying

the nozzle starting. See [8] for the *classical* model of the nozzle starting process.

The useful test time is terminated by the arrival of driver gas at the nozzle exit. Generally, the mechanism used to model the premature driver-gas contamination of the test gas has been based on the interaction of the reflected shock with the boundary layer along the shock-tube wall [9]. However, in the simulations of the shock reflection process, an alternative mechanism is seen. Shortly after shock reflection, a vortex develops near the tube centreline and travels upstream with the reflected shock. This vortex enhances the mixing the fluid in the middle of the tube rather than along the tube walls.

2 NUMERICAL SIMULATION

The computations reported here were performed with a finite-volume upwind code based on the full Navier-Stokes equations. The code is described briefly here but further detail (including notation) is available in [10].

2.1 Governing Equations

For an axisymmetric flow (with y as the radial coordinate), the finite-volume formulation of the Navier-Stokes equations may be expressed as

$$\frac{d < U >}{dt} + \frac{1}{\Omega'} \int_S (yF - yF_v)\, dy - \frac{1}{\Omega'} \int_S (yG - yG_v)\, dx = Q' \tag{1}$$

where $< \bullet >$ indicates a volume average, Ω' is the volume per radian and S is a contour in the (x, y)-plane around the volume. The U, F and G vectors are

$$U = \begin{bmatrix} \rho \\ \rho u \\ \rho v \\ \rho E \end{bmatrix} , \quad yF = y \begin{bmatrix} \rho u \\ \rho u^2 + P \\ \rho vu \\ \rho Eu + Pu \end{bmatrix} , \quad yG = y \begin{bmatrix} \rho v \\ \rho uv \\ \rho v^2 + P \\ \rho Ev + Pv \end{bmatrix} . \tag{2}$$

Note that, except for the "y" premultiplying factor, they are the same as those in the planar two-dimensional situation. The viscous terms are

$$yF_v = \begin{bmatrix} 0 \\ y\tau_{xx} \\ y\tau_{xy} \\ y\tau_{xx}u + y\tau_{xy}v + yq_x \end{bmatrix} , \quad yG_v = \begin{bmatrix} 0 \\ y\tau_{yx} \\ y\tau_{yy} \\ y\tau_{yx}u + y\tau_{yy}v + yq_y \end{bmatrix} , \tag{3}$$

where

$$\tau_{xx} = 2\mu \frac{\partial u}{\partial x} + \lambda \left(\frac{\partial u}{\partial x} + \frac{\partial v}{\partial y} + \frac{v}{y} \right) , \quad \tau_{yy} = 2\mu \frac{\partial v}{\partial y} + \lambda \left(\frac{\partial u}{\partial x} + \frac{\partial v}{\partial y} + \frac{v}{y} \right) , \quad \tau_{xy} = \tau_{yx} = \mu \left(\frac{\partial u}{\partial y} + \frac{\partial v}{\partial x} \right) , \tag{4}$$

and

$$q_x = -k\frac{\partial T}{\partial x} \quad , \quad q_y = -k\frac{\partial T}{\partial y} \quad . \tag{5}$$

Treating the viscous contributions in the form $y\tau$ avoids any difficulties with the geometry singularity at $y = 0$. The *effective* source term is

$$Q' = \begin{bmatrix} 0 \\ 0 \\ (P - \tau_{\theta\theta})A/\Omega' \\ 0 \end{bmatrix} \quad , \text{ where } \tau_{\theta\theta} = 2\mu\frac{v}{y} + \lambda\left(\frac{\partial u}{\partial x} + \frac{\partial v}{\partial y} + \frac{v}{y}\right) \quad . \tag{6}$$

To augment these equations, we use the equation of state for a calorically perfect gas

$$P = \rho(\gamma - 1)e \quad , \tag{7}$$

Sutherland's viscosity expression (to obtain $\mu = \mu(T)$), Stokes' hypothesis $\lambda = -\frac{2}{3}\mu$ and a constant Prandtl number.

2.2 Numerical Implementation

The flow domain in the (x, y)-plane is discretized as a structured mesh of quadrilateral cells with flow properties stored at the cell centres. At each time step, the inviscid-flux vectors (2) are evaluated by first applying a MUSCL interpolation scheme to obtain "left" and "right" states at the midpoints of the cell interfaces. A locally one-dimensional (approximate) Riemann solver is then applied to obtain the interface flow properties during the time step. The spatial derivatives used in the viscous flux vectors (3)-(5) are obtained at the cell vertices by applying the divergence theorem. The source term (6) is evaluated at the cell centres. The line integrals in (1) are then evaluated using the midpoint rule and the solution advanced in time with an Euler scheme or a predictor-corrector scheme.

2.3 Flow Geometry and Initial Conditions

The flow domain used in these calculations included a $1.5m$-long section of the shock tube, a transition region into the throat and a Mach 8 nozzle. Fig. 2 shows the shock-reflection region and nozzle throat while the coordinates for key points are given in Table 1. The nozzle expansion consists of a conical section from $x = 0$ to $x = 0.168m$ followed by a contoured wall which straightens the flow (with the aim of producing a uniform and parallel test flow near the nozzle exit plane). The contoured wall is specified as a cubic spline with the knots given in Table 2.

The grids were generated as single-block structured grids. That is, a single pair of i, j indices was used to address cells throughout the domain. This resulted in some mesh distortion in the transition region between the shock tube and the nozzle throat. Cases run on a range of grid

resolutions, however, indicated that the mesh distortion had little effect upon the computed results. Starting at the entrance to the throat, cells were clustered toward the nozzle wall in order to resolve the boundary layer. No attempt was made to resolve the boundary layer in the shock tube or in the shock-reflection region. In the axial direction, cells were clustered toward the nozzle throat.

Although the actual test gas used in the facility was air and the temperatures were high enough for chemical effects to be significant, the calculations presented here were run with a constant ratio of specific heats. A value of $\gamma = 1.3$ was used in order to approximate some of the high temperature effects. The gas constant was $R = 287\ J/kg/K$ and the Prandtl number was $Pr = 0.72$. Note that the driver gas was not included in these simulations.

To approximate conditions discussed in [6], the initial state of the gas in the shock tube was set to

$$P_1 = 75.0 \times 10^3\ Pa,\ \ \rho_1 = 0.9679\ kg/m^3,\ \ u_1 = 0\ m/s,\ \ T_1 = 270\ K,\ \ e_1 = 0.2583 \times 10^6\ J/kg,$$

and a post-shock condition of

$$P_2 = 5.812 \times 10^6\ Pa,\ \ \rho_2 = 6.764\ kg/m^3,\ \ u_2 = 2254 m/s,\ \ T_2 = 2994\ K,\ \ e_2 = 2.864 \times 10^6\ J/kg,$$

was applied to the inflow plane ($x = -1.5m$). This resulted in a primary shock Mach number $M_1 = 8.29$ and speed $W_1 = 2630 m/s$. At $t = 0$, the primary shock was located at $x = -0.101m$. For ideal reflection, the stagnation conditions (between the reflected shock and the closed end of the tube) would have been

$$P_s = 51.05 \times 10^6\ Pa,\ \ T_s = 6330\ K,\ \ \rho_s = 28.10\ kg/m^3,$$

with a reflected-shock speed of $W_R = 714\ m/s$. The total enthalpy in the stagnation region was $H_s = 7.87 \times 10^6 J/kg$. If the gas was allowed to expand isentropically to sonic conditions, the nominal throat conditions would have been

$$P_* = 27.86 \times 10^6\ Pa,\ \ \rho_* = 17.64\ kg/m^3,\ \ u_* = 1433\ m/s,\ \ T_* = 5504\ K,\ \ e_* = 5.266 \times 10^6\ J/kg\ .$$

Bursting of the secondary diaphragm (located at $x = 0$) was modelled by running the simulation in two stages. In the first stage, the primary shock was allowed to propagate to through the throat with pre-shock conditions applied as initial conditions throughout the nozzle expansion. As soon as the primary shock propagated into the nozzle expansion, the simulation was stopped and the flow state in the nozzle expansion (i.e. $0 < x < 2.187\ m$) was reset to

$$P_i = 32.7\ Pa,\ \ \rho_i = 3.833 \times 10^{-4}\ kg/m^3,\ \ u_i = 0\ m/s,\ \ T_i = 296\ K,\ \ e_i = 0.2832 \times 10^6\ J/kg\ .$$

These conditions approximated the "evacuated" conditions found in the experimental facility.

3 RESULTS

3.1 Nozzle Starting Process

Fig. 3 shows the evolution of the density field on a 600×80 mesh. The simulation starts at $t = 0$ with the primary shock propagating toward the throat. By $t = 0.1\ ms$, the reflected shock is established and is bringing the test gas to rest upstream of the throat. Simultaneously, some of the stagnant test gas is expanding through the throat and into the divergent section of the nozzle.

The essential features of the nozzle starting process are well described by quasi-one-dimensional model presented in [8]. As the primary shock travels down the nozzle it accelerates into the very low pressure gas already in the nozzle but, because of the diverging nozzle walls, it subsequently decelerates. Test gas which accelerates through the nozzle throat following the primary shock, expands to a very high Mach number and is suddenly decelerated when it encounters the slower primary shock structure. An upstream-facing shock is thus formed and is swept downstream through the nozzle. Although the primary shock remains essentially planar, the contact surface between it and the upstream-facing shock undergoes a Rayleigh-Taylor (or Richmyer-Meshkov) type of instability and becomes quite distorted. The upstream-facing shock becomes slightly distorted but remains essentially coherent.

Between the upstream-facing shock and the steady expansion being established near the throat there is an unsteady expansion, the upstream head of which is being swept downstream with velocity $u-a$. The unsteady expansion can be identified in Fig. 3 by the turning out of the contours between the upstream-facing shock and the nozzle throat. The unsteady expansion is the last wave to be expelled from the nozzle and by $t = 1.2\ ms$ the flow near the exit plane is approaching steady state.

Fig. 4 shows the normalized Pitot profile (at late times) compared with experimental measurements from [6]. The key feature of the profiles is that they are all reasonably flat in the test core region. However, the computed boundary layer is too thin and consequently the average value of computed Pitot pressure in the core flow is lower than that measured in the experiment. The simulated and experimental Pitot pressure histories for three radial locations near the nozzle exit plane are shown in Fig. 5. The timimg of the passage of the upstream-facing shock and of the unsteady expansion closely agree but, the large disturbance seen in the experimental measurements for $0.7\ ms < t < 1.0\ ms$ at $x \simeq 0.006$ is not present in the simulation results.

3.2 Shock Reflection Process

Although the scale of Fig. 3 is very small, it is clear that the reflected shock is not planar. At late times (i.e. $t > 0.4\ ms$), this may be caused by inadequate grid resolution but, at earlier times, a complex structure is developed consistently for a range of grid resolutions. Fig. 6 shows a more detailed evolution of the density field in the shock-reflection region. To focus on events in the shock-

reflection (or nozzle-supply) region, the flow domain is restricted to $-0.20m \leq x \leq 0.01m$ and is discretized as a mesh of 300 × 100 cells. The sequence begins at $t = 0.030\ ms$ with the reflected shock just beginning to move away from the flat end of the shock tube. Near the centreline, the primary shock continues to propagate downstream through the throat. At $t = 0.040\ ms$, the reflected shock has moved further upstream and fluid which has been brought to rest behind the reflected shock begins to accelerate toward the tube axis and into the throat. Near the entrance to the throat ($x \simeq -0.025m$, $y \simeq 0$), a vortex is created and, in subsequent frames, continues to grow and follow the reflected shock. By $t = 0.20\ ms$, the vortex has weakened and the reflected shock has become nearly plane. Note that this has not been observed in either experiment or simulation in two-dimensional flow. Fig. 7 shows the velocity field at an intermediate state and it can be seen that the vortex entrains fluid near the tube centreline well into the nozzle supply region. Hence, in the presence of a contact surface between driver gas and test gas (which is expected to be nearby for high-enthalpy operating conditions), this mechanism may cause premature contamination of the test gas.

4 CONCLUDING REMARKS

This paper has examined the shock-reflection and nozzle starting processes encountered in a reflected-shock tunnel. The simulation of the nozzle starting process did agree with the experimental data with respect to the timing of various events but did not identify the late-time disturbances seen in the experimental data. Obvious flaws in the simulation include, the lack of a turbulence model, and the omission of the driver gas and high-temperature chemical effects.

The simulations did, however, identify a novel mechanism for the premature contamination of the test gas and may complement the traditional modelling of the interaction of the reflected shock with the shock-tube boundary layer [9]. This mechanism is based on the establishment and propagation of a vortex near the centre of the shock tube and just behind the reflected shock. Presently, this simulation has been done for only one operating condition, with a perfect gas, and with no boundary layers on the shock tube walls. More work needs to be done to investigate the mechanism in the presence of a driver-gas/test-gas interface and to find the range of operating conditions over which the mechanism is expected to be important.

References

[1] R. J. Stalker. *Annual Review of Fluid Mechanics*, 21:37-60, 1989.

[2] N. R. Mudford, R. J. Stalker, and I. Shields. *Aeronautical Quarterly*, May.113-131, 1980.

[3] H. G. Hornung and J. Belanger. AIAA Paper 90-1377, 1990.

[4] V. L. Gregorenko, A. M. Naumov, and N. I. Hvostor. *Scientific Notes of the Central Hydrodynamic Institute*, 15(5), 1984.

[5] A. B. Britan and E. I. Vasil'ev. *Izvestiya Academii Nauk SSSR*, 5:88–95, 1986.

[6] P. A. Jacobs. AIAA Paper 91-0295, 1991.

[7] Y. Byun, J. Y. Lee, J. D. Anderson, and A. P. Kothari. AIAA Paper 90-0421, 1990.

[8] C. E. Smith. *Journal of Fluid Mechanics*, 24:625–640, 1966.

[9] L. Davies and J. L. Wilson. *The Physics of Fluids Supplement 1*, pages I-37 - I-43, 1969.

[10] P. A. Jacobs. ICASE Interim Report 18, 1991.

label	x, m	r, m	comment
a_1	-1.5	0.0	inflow plane
a_2	-1.5	0.038	
b_1	-0.101	0.0	start grid distortion
b_2	-0.101	0.038	
c_1	-0.063	0.0	turn grid 90°
c_2	-0.025	0.038	
d_1	-0.04262	0.0	
d_2	-0.025	0.01762	start radius into throat
e_1	-0.015	0.0	start of constant area throat
e_2	-0.015	0.00762	
f_1	0.0	0.0	end of throat
f_2	0.0	0.00762	start of conical expansion

Table 1: Points defining the shock-reflection region and nozzle throat.

j	x_j, m	y_j, m	comment
1	0.16800	0.04951	end of cone, $dy/dx = 0.2493$
2	0.45648	0.10584	
3	0.74488	0.14208	
4	1.03336	0.16552	
5	1.32176	0.18104	
6	1.61024	0.19040	
7	1.89872	0.19520	
8	2.18712	0.19688	end of nozzle wall

Table 2: Knots for the cubic interpolating spline for the Mach 8 nozzle wall.

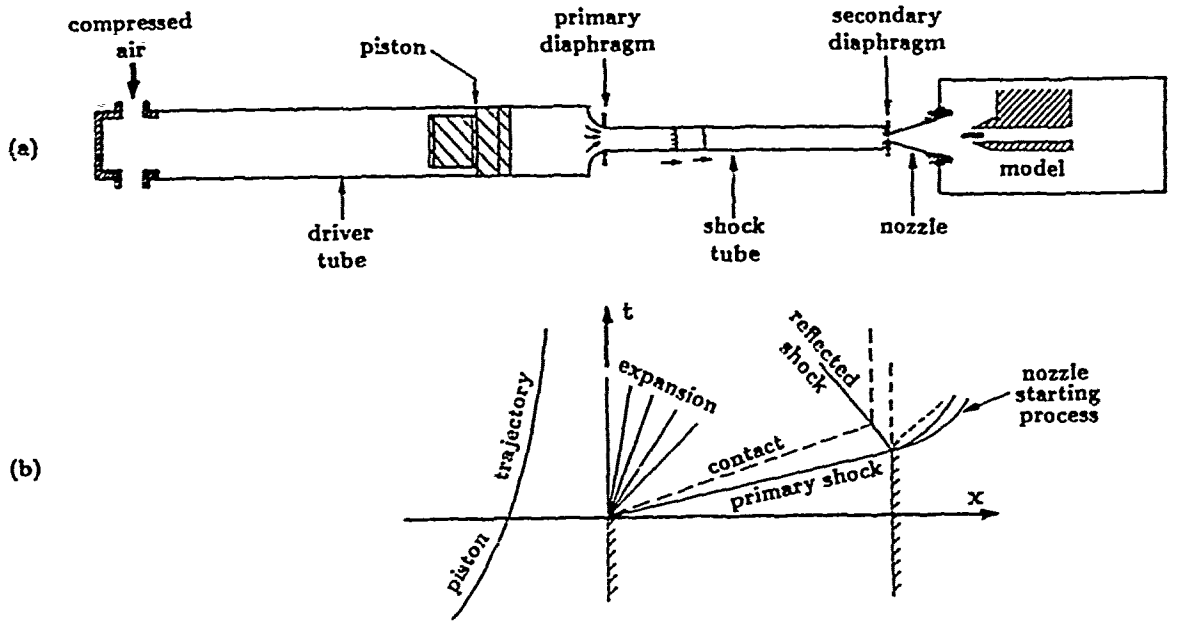

Figure 1: Reflected-shock tunnel operation. (a) Tunnel schematic; (b) $x - t$ wave diagram.

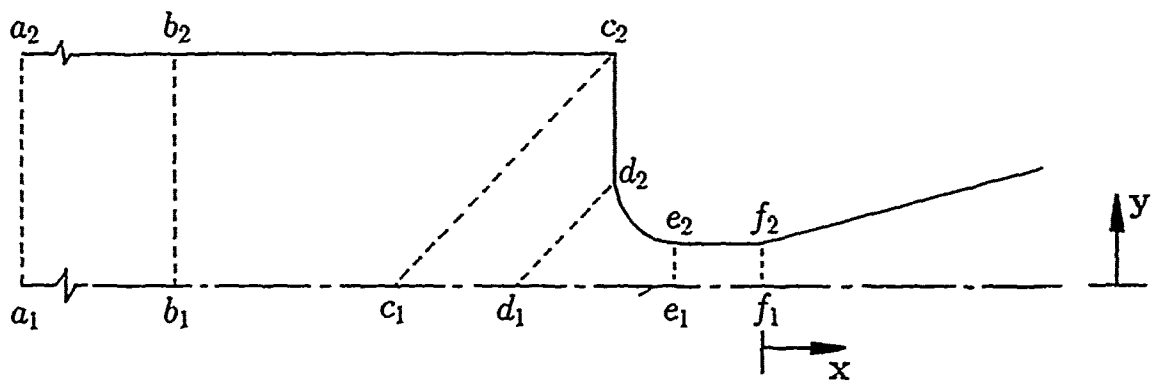

Figure 2: Geometry for the shock-reflection region.

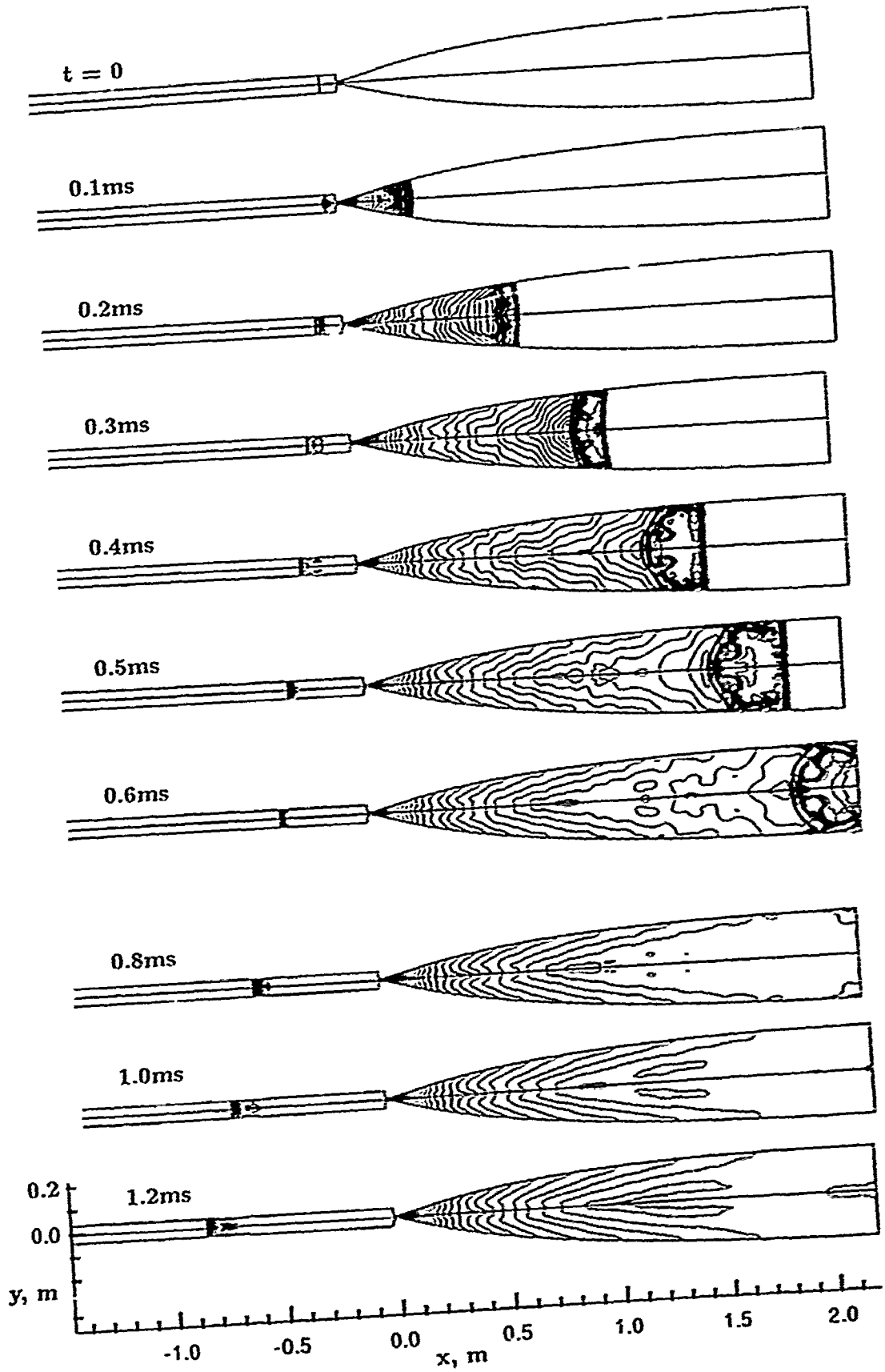

Figure 3: Evolution of the density field ($\log_{10}\rho$). Times as shown.

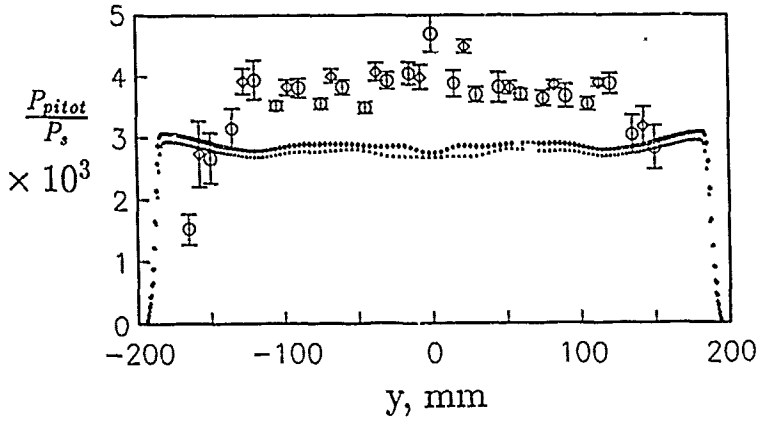

Figure 4: Normalized Pitot pressure profile at $x \simeq 1.8m$: ◯ = experiment; o = simulation at $t = 1.0ms$; △ = simulation at $t = 1.2ms$.

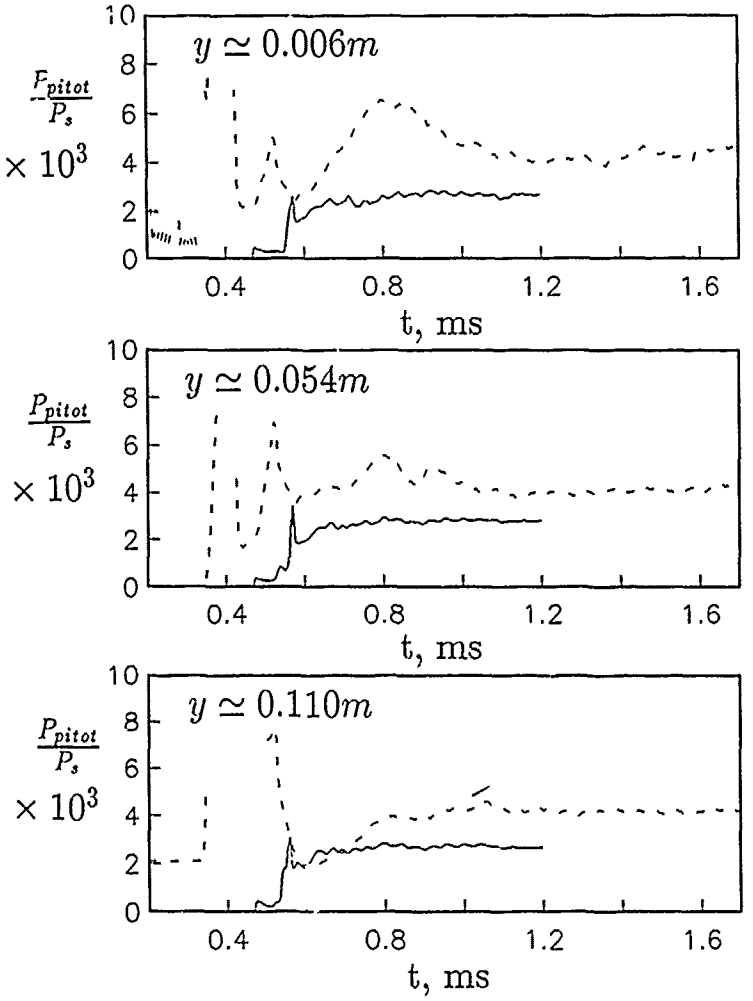

Figure 5: Evolution of the normalized Pitot pressure at $x \simeq 1.8m$: solid line = simulation; dashed line = experiment. Radial locations as shown.

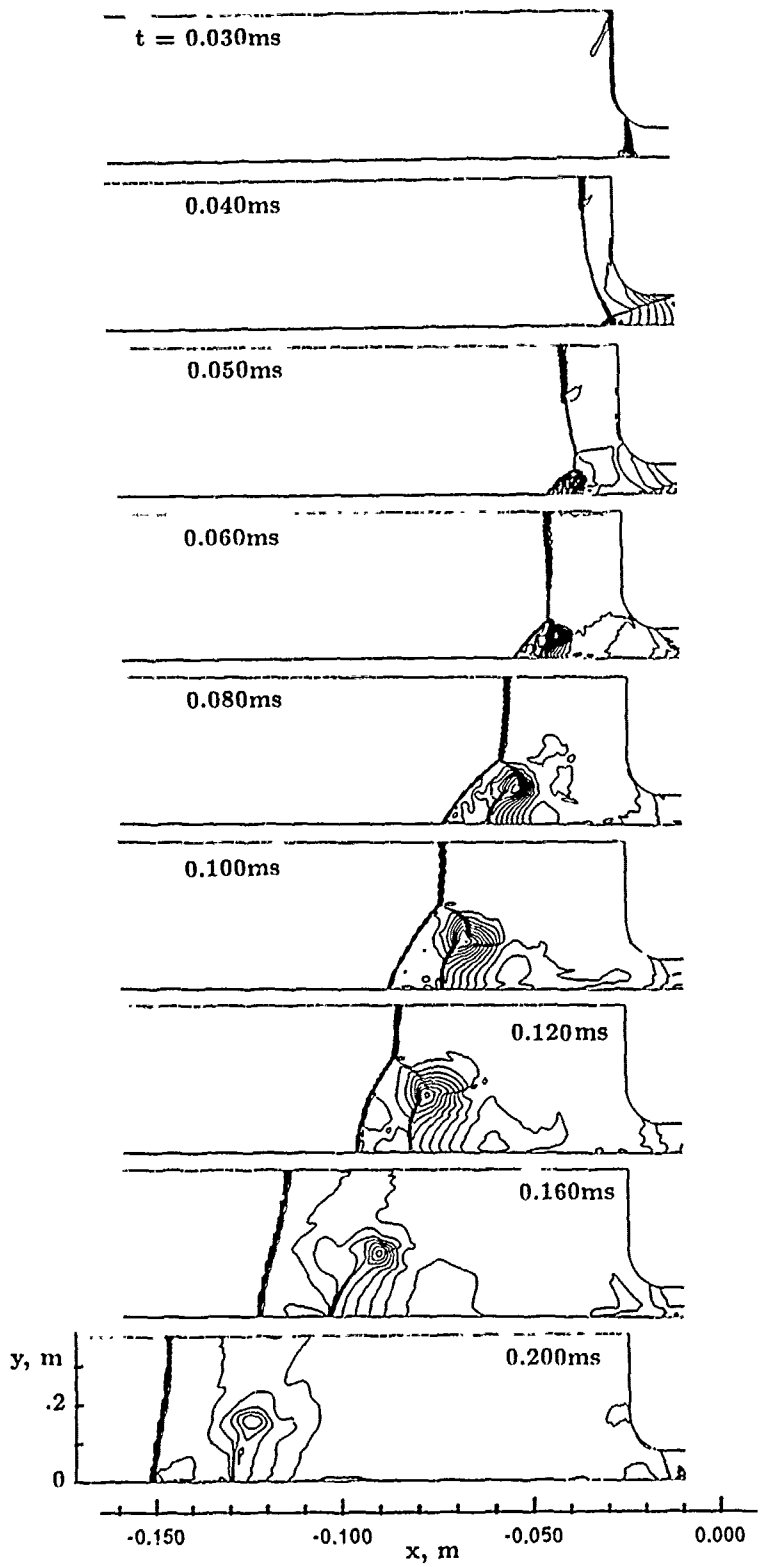

Figure 6: Evolution of the density field ($\log_{10}\rho$) in the shock-reflection region. Times as shown.

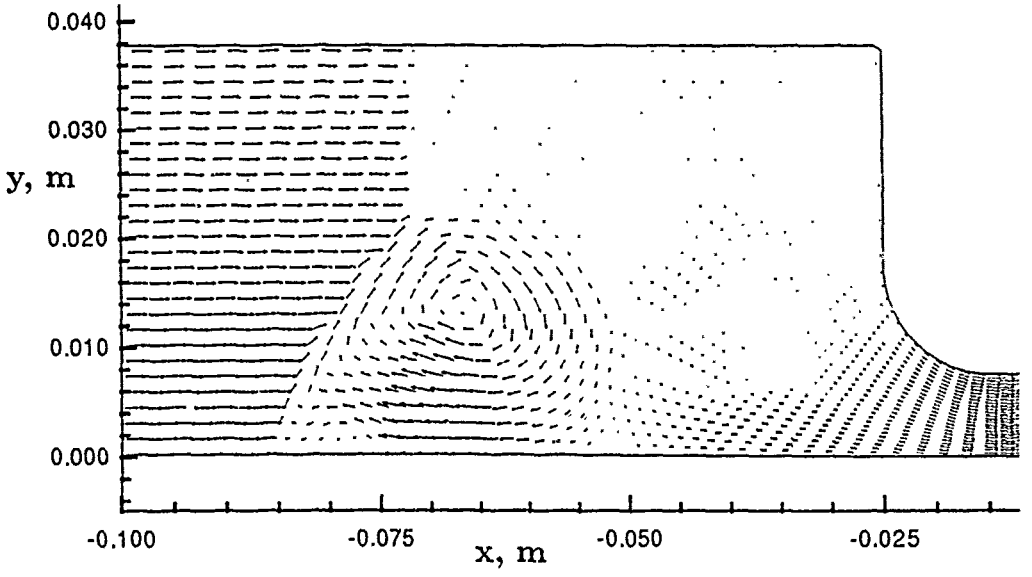

Figure 7: Velocity field in the shock-reflection region at $t = 0.10ms$.

NASA

Report Documentation Page

1. Report No.	2. Government Accession No.	3. Recipient's Catalog No.
NASA CR-187606 ICASE Report No. 91-60		

4. Title and Subtitle	5. Report Date
SIMULATION OF TRANSIENT FLOW IN A SHOCK TUNNEL AND A HIGH MACH NUMBER NOZZLE	July 1991
	6. Performing Organization Code
7. Author(s)	8. Performing Organization Report No.
P. A. Jacobs	91-60
	10. Work Unit No.
9. Performing Organization Name and Address	505-90-52-01
Institute for Computer Applications in Science and Engineering Mail Stop 132C, NASA Langley Research Center Hampton, VA 23665-5225	11. Contract or Grant No. NAS1-18605
	13. Type of Report and Period Covered
12. Sponsoring Agency Name and Address	Contractor Report
National Aeronautics and Space Administration Langley Research Center Hampton, VA 23665-5225	14. Sponsoring Agency Code

15. Supplementary Notes

Langley Techical Monitor:
Michael F. Card

Final Report

To be presented at the 4th International Symposium on Computational Fluid Dynamics, Davis, CA, Sept. '91

16. Abstract

A finite-volume Navier-Stokes code was used to simulate the shock-reflection and nozzle starting processes in an axisymmetric shock tube and a high Mach number nozzle. The simulated nozzle starting processes were found to match the classical quasi-one-dimensional theory and some features of the experimental measurements. The shock-reflection simulation illustrated a new mechanism for the driver-gas contamination of the stagnated test gas.

17 Key Words (Suggested by Author(s))	18. Distribution Statement
shock tunnel; Navier-Stokes simulation; Nozzle starting; shock reflection	09 - Research and Support Facilities (Air) 34 - Fluid Mechanics and Heat Transfer Unclassified - Unlimited

19 Security Classif. (of this report)	20 Security Classif (of this page)	21 No of pages	22 Price
Unclassified	Unclassified	15	A03

NASA FORM 1626 OCT 86